Comparison of the anisotropic-ray-theory rays and anisotropic common S-wave rays with the SH and SV reference rays in a velocity model with a split intersection singularity

Petr Bulant and Luděk Klimeš

Department of Geophysics, Faculty of Mathematics and Physics, Charles University, Ke Karlovu 3, 121 16 Praha 2, Czech Republic
(http://sw3d.cz/staff/bulant.htm, http://sw3d.cz/staff/klimes.htm)

Received: November 2, 2016; Revised: February 20, 2017; Accepted: March 11, 2017

ABSTRACT

We describe the behaviour of the anisotropic–ray–theory S–wave rays in a velocity model with a split intersection singularity. The anisotropic–ray–theory S–wave rays crossing the split intersection singularity are smoothly but very sharply bent. While the initial–value rays can be safely traced by solving Hamilton's equations of rays, it is often impossible to determine the coefficients of the equations of geodesic deviation (paraxial ray equations, dynamic ray tracing equations) and to solve them numerically. As a result, we often know neither the matrix of geometrical spreading, nor the phase shift due to caustics. We demonstrate the abrupt changes of the geometrical spreading and wavefront curvature of the fast anisotropic–ray–theory S wave. We also demonstrate the formation of caustics and wavefront triplication of the slow anisotropic–ray–theory S wave.

Since the actual S waves propagate approximately along the SH and SV reference rays in this velocity model, we compare the anisotropic–ray–theory S–wave rays with the SH and SV reference rays. Since the coupling ray theory is usually calculated along the anisotropic common S–wave rays, we also compare the anisotropic common S–wave rays with the SH and SV reference rays.

Keywords: wave propagation, elastic anisotropy, heterogeneous media, anisotropic ray theory, geodesic deviation, phase shift due to caustics, two–point ray tracing, S–wave singularities

1. INTRODUCTION

In a generally anisotropic medium, we may define various kinds of reference rays which may but need not approximate the actual wave paths, and thus may but need not be applicable to the study of wave propagation. For a better physical insight, it is thus desirable to demonstrate the advantages and weaknesses of various kinds of reference rays using numerical examples. In this paper, we compare various kinds of reference rays in velocity model SC1_II (*Pšenčík et al., 2012*) with a split intersection singularity.

For two–point ray tracing in heterogeneous media, we need *ray histories* (*Bulant, 1996*; *Vinje et al., 1996, p. 824*; *Červený et al., 2007, Sec. 2.2*), which may be indexed by integers. Rays of the same ray history pass through an equal sequence of blocks and interfaces and terminate at an equal reference surface. Each sequence of blocks and interfaces encountered during ray tracing thus defines the corresponding ray history. The ray history may or may not include the *KMAH index*, which determines the phase shift due to caustics. A KMAH index of +1 indicates a phase shift of the complex–valued amplitude by $\pi/2$ in the direction corresponding to increasing *time* (or decreasing *travel time*) of the time–harmonic wave (*Klimeš, 2010*, *2014*).

In a generally anisotropic medium, the S–wave slowness sheets of the slowness surface are usually mostly separated and intersect in as many as 32 S–wave point singularities (*Vavryčuk, 2005a,b*). In this case, outside the point singularities, the anisotropic–ray–theory rays (*Babich, 1961*; *Červený, 2001*) stay at the fast or slow S–wave slowness sheet, respectively. When approaching the point singularities, the limiting case again corresponds to staying at the fast or slow S–wave slowness sheet, respectively. In a generally anisotropic medium, we thus have to separate the slowness surface into the P–wave slowness sheet, the fast S–wave slowness sheet and the slow S–wave slowness sheet.

However, in a transversely isotropic medium, the S–wave slowness sheets may intersect along intersection singularities (*Vavryčuk, 2003b*). In this special case, we can separate the slowness surface into the P–wave slowness sheet, the SH–wave slowness sheet and the SV–wave slowness sheet, and trace the SH and SV rays. We must know a priori whether the medium is transversely isotropic. We cannot determine it numerically, because any rounding error can perturb a transversely isotropic medium to a generally anisotropic medium and split the unstable intersection singularity (*Crampin, 1981*) which disappears or is transformed into point singularities.

If a medium is close to transversely isotropic, but is not transversely isotropic, the intersection singularity disappears, the slow S–wave slowness sheet separates from the fast S–wave slowness sheet, forming smooth but very sharp edges on both sheets. This geometry is referred to as the *split intersection singularity*.

When the slowness vector of a ray passes smoothly through a split intersection singularity, or near a conical or wedge singularity, the ray–velocity vector rapidly changes its direction and creates a sharp bend of the ray, see Fig. 2. This sharp bend is connected with a rapid rotation of the eigenvectors of the Christoffel matrix

(*Vavryčuk, 2003a*). The sharply bent rays thus cannot describe the correct wave propagation and indicate a failure of the anisotropic ray theory. Refer to *Bulant and Klimeš (2017, Sec. 1.2)* for a more detailed description of the problem of split intersection singularities including illustrations. The problem of sharply bent rays near conical or wedge singularities is analogous.

Klimeš and Bulant (2014a) have demonstrated that the physically reasonable anisotropic–ray–theory rays represent better reference rays for calculating the corresponding arrivals of the prevailing frequency approximation of the coupling ray theory (*Klimeš and Bulant, 2012*, *2016*) than the anisotropic common S–wave rays. However, the sharply bent rays are worse reference rays than the anisotropic common S–wave rays, see Figs 9–14 in which the SH and SV reference rays represent good approximations of the actual wave paths (*Klimeš and Bulant, 2015*, *2017*).

On the one hand, the sharply bent anisotropic–ray–theory S–wave rays can safely be traced by solving Hamilton's equations of rays for given initial conditions. On the other hand, the dependence of the second derivatives of the Hamiltonian function with respect to the slowness vector along the ray contains a narrow spike resembling a Dirac distribution. This narrow spike destroys the numerical integration of the equations of geodesic deviation (paraxial ray equations, dynamic ray tracing equations), and the matrix of geometrical spreading becomes random beyond the spike. Moreover, numerical integration can generate several spurious changes of the signature of the matrix of geometrical spreading, which may result in various incorrectly large KMAH indices. Random incorrect KMAH indices cannot be used to determine ray histories during two–point ray tracing. Even if we remove the KMAH index from the ray histories, we cannot use the randomly generated matrix of geometrical spreading for two–point ray tracing.

In this paper, we shall present examples of the sharply bent anisotropic–ray–theory rays in velocity model SC1_II which contains a split intersection singularity. We demonstrate numerically the problems with two–point ray tracing of the anisotropic–ray–theory S–wave rays. We simultaneously demonstrate the smooth and reasonable behaviour of the anisotropic common S–wave rays which are usually used as the reference rays for the coupling ray theory. Since the actual S waves propagate approximately along the SH and SV reference rays in this velocity model, we also compare the anisotropic–ray–theory S–wave rays and the anisotropic common S–wave rays with the SH and SV reference rays. The problems studied in this paper are both fundamental (e.g., incorrect reference amplitudes) and numerical (e.g., impossibility to calculate the reference amplitudes).

Velocity model SC1_II was used by *Pšenčík et al. (2012)* and *Bulant et al. (2011)* to compare synthetic seismograms calculated by different ray theories with the seismograms calculated by the Fourier pseudospectral method. Since the phase–velocity section shown by *Pšenčík et al. (2012, Fig. 11)* indicated the possible existence of the split intersection singularity above the original surface of the velocity model, we decided to extend the velocity model in the vertical direction, and have added 13 new receivers above the original vertical receiver profile.

2. VELOCITY MODEL SC1_II

The matrix of the density–normalized elastic moduli in velocity model SC1_II is prescribed at depths of 0 km and 1.5 km (*Pšenčík et al., 2012, Eq. 19*), and is linearly interpolated with respect to depth. At the depth of 0 km, velocity model SC1_II is approximately transversely isotropic with a tilted axis of symmetry (*Klimeš, 2015*, *2016*), and the slowness surface contains a split intersection singularity. At the depth of 1.5 km, velocity model SC1_II is very close to isotropic, but is slightly cubic and its symmetry axes coincide with the coordinate axes. This means that velocity model SC1_II is very close to transversely isotropic at all depths, but is slightly tetragonal.

The S–wave anisotropy in the velocity model, defined as $2(p_{\max}-p_{\min})/(p_{\max}+p_{\min})$ where $p_{\max}$ and $p_{\min}$ are the maximum and minimum lengths of the slowness vector, is 8.5% for the slow wave and 11.2% for the fast wave at the depth of 0 km, and 4.5% for the slow wave and 5.9% for the fast wave at the depth of 0.5 km.

The slowness surface at the depth of 0.5 km is displayed in Fig. 1. Whereas the transversely isotropic medium contains the intersection singularity through which the rays pass without rotation of the eigenvectors of the Christoffel matrix (*Vavryčuk, 2001, Sec. 4.3*), in the slightly tetragonal medium, the S–wave slowness surface is split at this unstable singularity (*Crampin, 1981*) and the eigenvectors of the Christoffel matrix rapidly rotate by 90° there.

3. ANISOTROPIC–RAY–THEORY S–WAVE RAYS IN VELOCITY MODEL SC1_II

3.1. Initial–value tracing of anisotropic–ray–theory S–wave rays

We use SW3D software package CRT version 7.10 (*Bucha and Bulant, 2014*) to calculate anisotropic–ray–theory S–wave rays. Tracing of anisotropic–ray–theory S–wave rays is designed for general anisotropy with S–wave point singularities only, and the type of traced wave (the fast S wave or the slow S wave) is chosen a priori. In each step of ray tracing, the Christoffel matrix is calculated together with its eigenvalues and eigenvectors. We then select the a priori chosen S wave and calculate the ray.

The initial–value rays of the selected anisotropic–ray–theory S wave can be traced safely by solving Hamilton's equations of rays. Unfortunately, the equations of geodesic deviation (paraxial ray equations, dynamic ray tracing equations) contain second–order derivatives of the Hamiltonian function with respect to the slowness vector. Expressions for these derivatives contain the difference of the S–wave eigenvalues of the Christoffel matrix in the denominator. If the difference of the S–wave eigenvalues of the Christoffel matrix is smaller than the rounding error, the second–order derivatives of the Hamiltonian function with respect to the slowness vector become random and, in consequence, the matrix of geometrical spreading becomes random, too. If we require rays to have a reasonably defined matrix of geometrical

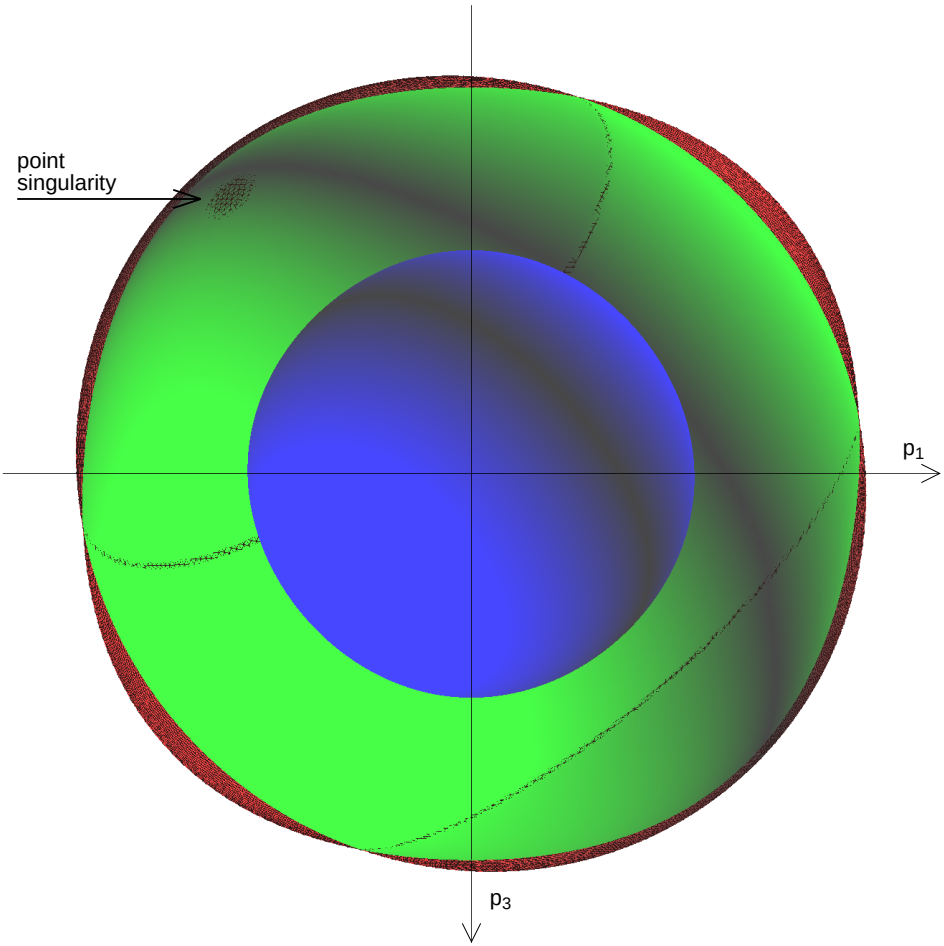

Fig. 1. Slowness surfaces in velocity model SC1_II at the depth of 0.5 km. The figure shows the halves of the slowness surfaces cut in the p_1–p_3 plane; we thus see the hemispheres of the slowness surfaces of the P wave (**blue**), fast S wave (**green**), and slow S wave (**red**). The red slowness surface of the slow S wave is covered by small triangles, and these triangles penetrate through the green slowness surface of the fast S wave at the places where the two surfaces are very close to each other. We thus see two half circles corresponding to the split intersection singularities, and a circular area corresponding to the point singularity in the left upper part of the figure (marked by an arrow).

spreading and a reasonably defined phase shift due to caustics, the ray tracing has to be terminated when the relative difference between the S–wave eigenvalues of the Christoffel matrix is smaller than a prescribed limit hereinafter denoted as *DS*. The maximum angular numerical error of the eigenvectors of the Christoffel matrix in radians is then roughly equal to the ratio of the relative rounding error to this parameter *DS*.

3.2. Source–receiver configuration

The point source is located at a depth of 0 km. We calculate rays approximately reaching the receivers located in a vertical well at a distance of 1 km from the source. The receivers extend from a depth of 1.32 km below the source to an elevation of 0.48 km above the source with a spacing of 0.04 km. *Klimeš and Bulant (2012, 2016)* considered the 33 receivers below the source. In this paper, we added a receiver at the source level and 12 receivers above the source in order to demonstrate the sharp bends of the S–wave anisotropic–ray–theory rays and the wavefront triplication of the slow anisotropic–ray–theory S–wave, see Fig. 2.

3.3 Problems of tracing the anisotropic–ray–theory S–wave two–point rays

We chose the value 10^{-5} of parameter *DS* mentioned above and traced the initial–value rays of the slow S wave. The ray parameters of the rays are displayed in Fig. 3, where the ray parameters are colour–coded and symbol–coded according to the *ray history* (*Bulant, 1996*). The rays of ray history 1 terminate at the surface of the velocity model, the rays of all other ray histories head for the right side of the velocity model which contains the receiver profile. The black plus crosses (ray history 2) correspond to the rays which do not touch a caustic and thus have KMAH index 0. The belt of other symbols roughly corresponds to the sharply bent rays (Fig. 2) which should have KMAH index 1. The yellow squares (ray history 5) indeed correspond to rays with KMAH index 1. We see that the boundary between KMAH index 0 and KMAH index 1 is not smooth, which means that the value of the KMAH index is sometimes incorrect for the chosen value of parameter *DS*. We also observe violet circles (ray history 6) corresponding to the rays with the incorrect value 2 of the KMAH index. The value 10^{-5} of parameter *DS* is thus too small for the correct determination of the matrix of geometrical spreading and of the KMAH index. However, the green x crosses (ray history 3, KMAH=0) and blue diamonds (ray history 4, KMAH=1) correspond to the rays whose tracing has been terminated due to the relative difference of the S–wave eigenvalues being smaller than $DS{=}10^{-5}$. The rays, whose tracing has been terminated completely, cover the region of the two–point rays corresponding to the reverse branch of the wavefront triplication, refer to Figs 2, 5 and 6. If we wish to obtain these two–point rays, we have to decrease the value of parameter *DS* considerably, although we know that the matrix of geometrical spreading and the KMAH index will then become random.

We thus chose the value 10^{-11} of parameter *DS* and traced the initial–value rays of the slow S wave. The ray parameters of the rays are displayed in Fig. 4. There are no rays whose tracing had to be terminated due to the relative difference of the S–wave eigenvalues being smaller than *DS*. All the initial–value rays have thus been calculated, but with random values of the KMAH index. The random values of the KMAH index are 0 (ray history 2), 1 (ray history 3), 2 (ray history 4) and 4 (ray history 5).

During the two–point ray tracing according to *Bulant (1996, 1999)*, we have to determine the boundaries between regions of different ray histories, in this case

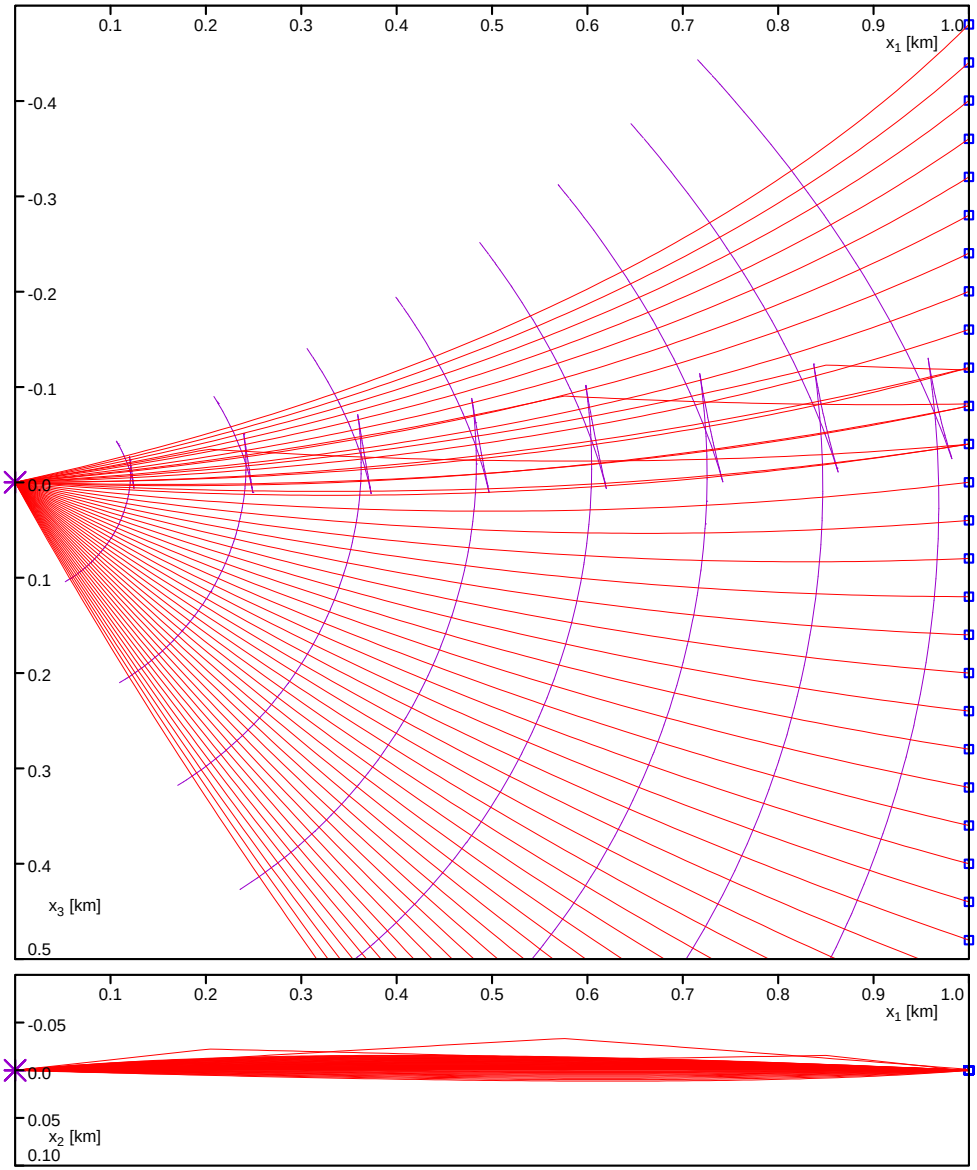

Fig. 2. Front view and top view of the anisotropic–ray–theory rays of the slow S wave. The front view is supplemented with the lines of intersection of the vertical source–receiver plane with the slow S–wave wavefronts at travel times 0.05, 0.10, 0.15, 0.20, 0.25, 0.30, 0.35 and 0.40 seconds. We can clearly observe the caustics caused by the sharply bent rays and the formation of the wavefront triplication at the first, second and third receivers above the source. We can observe that the sharply bent rays are significantly declined away from the source–receiver plane, while all the other rays almost stay at this plane. We can also observe that the first arrival at the triplication (concave part of the wavefront) has considerably lower geometrical spreading and thus higher amplitudes than the other two arrivals.

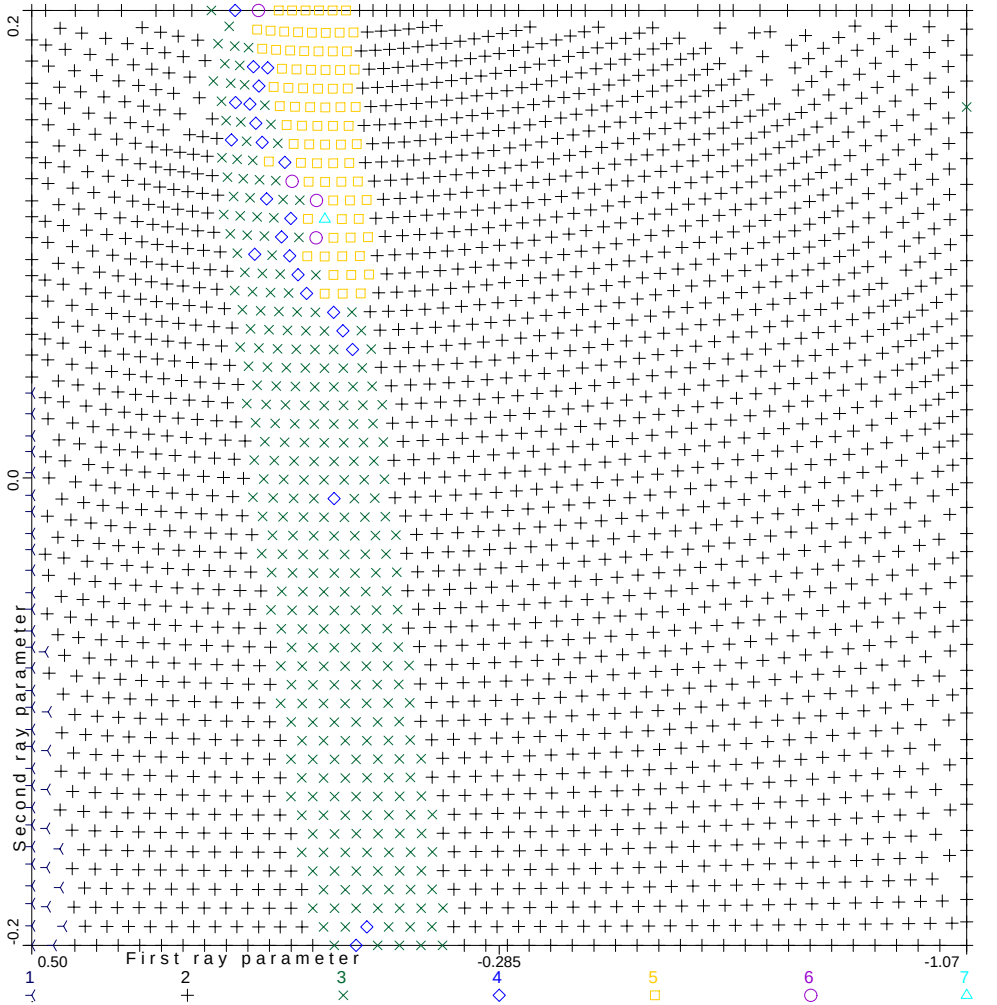

Fig. 3. Ray parameters of the basic system of the anisotropic–ray–theory rays of the slow S wave, traced with DS=10^{-5} and with the KMAH index included in the ray histories. The numbers and symbols plotted under the horizontal axis of the figure describe the colours and symbols used for the individual ray histories.

between the regions of different KMAH indices. The determination of the boundaries between the regions of random KMAH indices of Fig. 4, using additional auxiliary rays, again with random KMAH indices, obviously represents a disaster for the two–point ray tracing algorithm. The ray parameters of all anisotropic–ray–theory rays of the slow S wave traced with DS=10^{-11} during the two–point ray tracing are displayed in Fig. 5 together with the triangulation of the ray–parameter domain. The random values of the KMAH index are 0 (ray history 2), 1 (ray history 3), 2 (ray history 4), 3 (ray history 6), 4 (ray history 5), 5 (ray history 10), 6 (ray history 8)

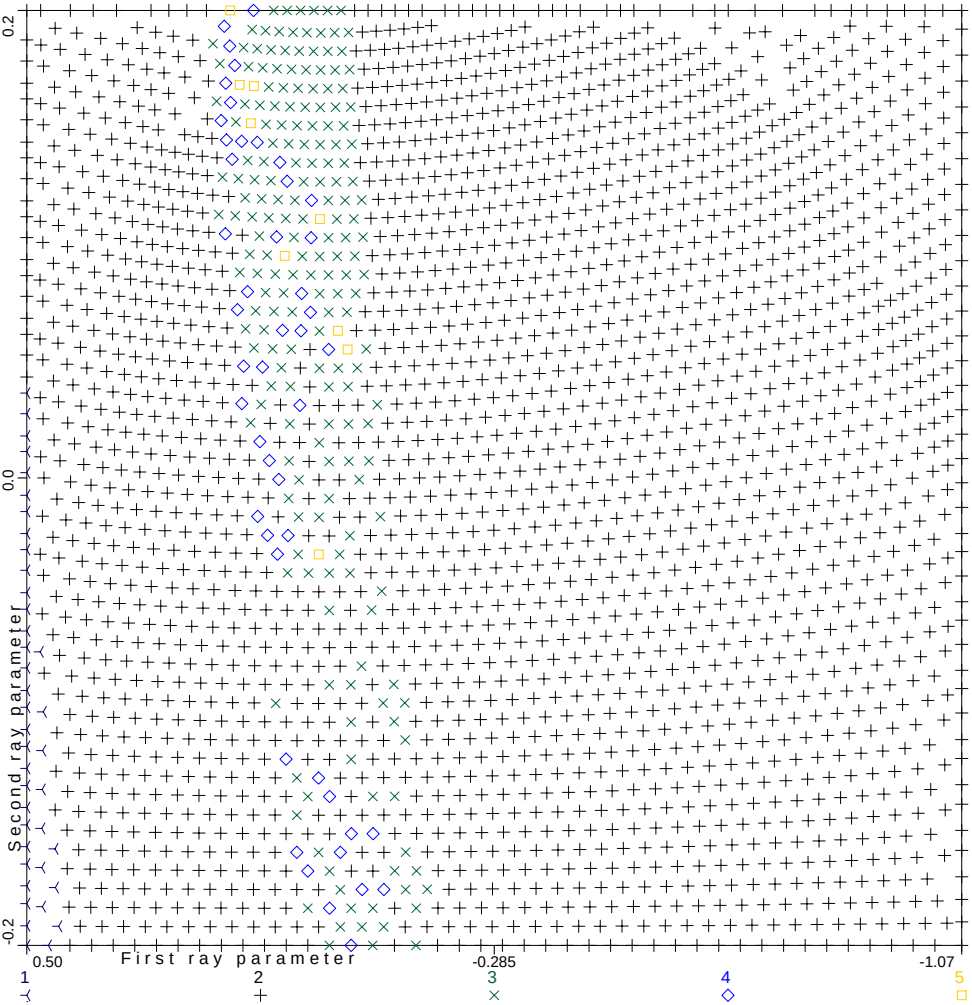

Fig. 4. Ray parameters of the basic system of the anisotropic–ray–theory rays of the slow S wave, traced with DS=10^{-11} and with the KMAH index included in the ray histories. Note that if these rays are traced with the KMAH index removed from the ray histories, ray histories 3–5 in this figure will change to ray history 2.

and 10 (ray history 9). Ray history 7 corresponds to the rays whose tracing has been terminated. The large red plus crosses correspond to the rays approximately reaching the receivers.

In order to trace the anisotropic–ray–theory rays of the slow S wave in velocity model SC1_II, we have optionally removed the KMAH index from the ray histories. The ray parameters of the initial–value rays, traced with DS=10^{-11} and with the KMAH index removed from the ray histories, correspond to Fig. 4 with ray histories 3–5 changed to ray history 2. In this case, there are no rays whose tracing had

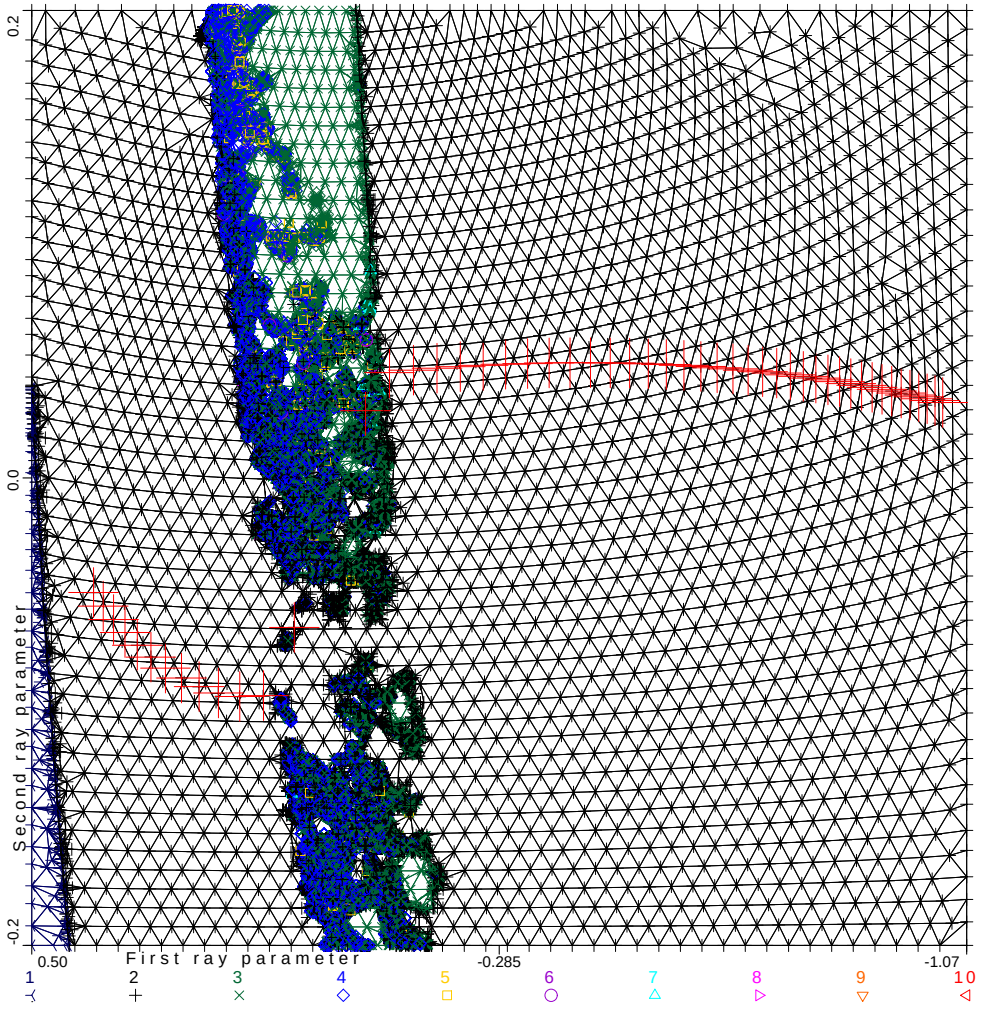

Fig. 5. Ray parameters of all traced anisotropic–ray–theory rays of the slow S wave, including the triangulation of the ray–parameter domain. The rays are traced with DS=10^{-11} and with the KMAH index included in the ray histories. The large red crosses correspond to the rays approximately reaching the receivers.

to be terminated, all the rays heading to the side of the velocity model containing the receiver profile have the same ray history 2. In this way, we can find the rays approximately reaching the receivers, see Fig. 6.

The corresponding slow S–wave rays are displayed in Fig. 2. Due to the constant vertical gradient of elastic moduli, the slowness vectors slowly rotate during ray tracing. The slowness vectors of the rays reaching the first, second, and the third receiver above the source cross the split intersection singularity. Crossing the split intersection singularity results in smooth but very sharp bends of rays. These sharp

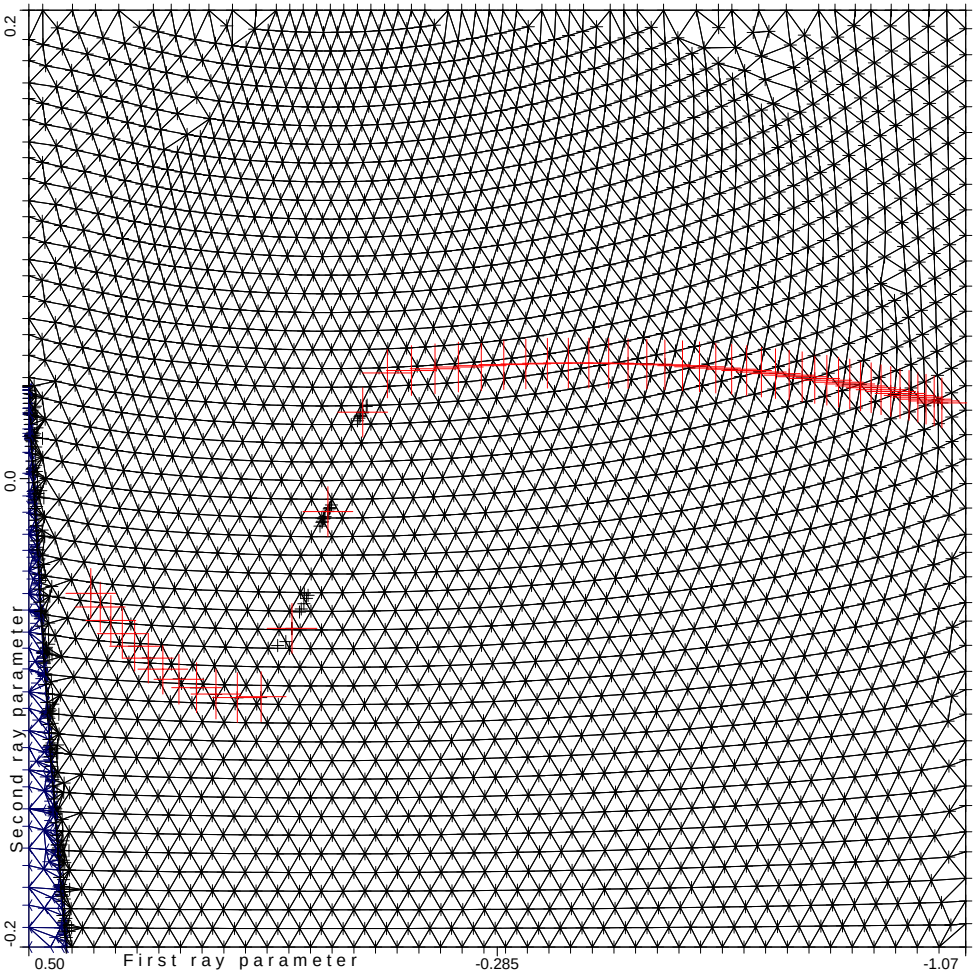

Fig. 6. Ray parameters of all traced anisotropic–ray–theory rays of the slow S wave, including the triangulation of the ray–parameter domain. The rays are traced with DS=10^{-11} and with the KMAH index removed from the ray histories. The large red crosses correspond to the rays approximately reaching the receivers. It is obvious from the distribution of the auxiliary rays shot towards the receivers that the paraxial approximation inevitably failed in the belt of sharply bent rays.

bends are connected with a rapid rotation of the eigenvectors of the Christoffel matrix. The sharply bent rays thus cannot describe the correct wave propagation and indicate a failure of the anisotropic ray theory, refer to *Pšenčík et al. (2012)* for numerical examples. The sharply bent slow S–wave rays form the wavefront triplication. The caustics limiting the triplication are positioned between the zeroth and first receivers above the source, and between the third and fourth receivers above the source, respectively.

The fast S–wave rays are displayed in Fig. 7. The sharply bent rays reach the receivers from the second receiver below the source to the ninth receiver above the source. These rays are bent in the opposite direction than the slow S–wave rays, causing an abrupt change of the amplitude between the second and third receivers below the source (and also between the ninth and tenth receivers above the source), which also suggests that the anisotropic ray theory is not applicable there.

Although we have finally determined the two–point rays in this case, they are of little practical value because the corresponding amplitudes and KMAH indices are not only inaccurate but are often random. The actual S wave does not propagate along these anisotropic–ray–theory two–point rays.

4. ANISOTROPIC COMMON S–WAVE TWO–POINT RAYS

The anisotropic common S–wave rays, traced using the average S–wave Hamiltonian function according to *Klimeš (2006)* are displayed in Fig. 8. The corresponding geometrical spreading and the corresponding amplitude are very smooth. There is thus no problem with two–point tracing the anisotropic common rays. Unfortunately, the corresponding smooth reference amplitude, common for both waves, differs from the correct amplitudes of the actual waves (*Klimeš and Bulant, 2015*, *2017*).

5. COMPARISON WITH THE SH AND SV REFERENCE RAYS

Since velocity model SC1_II is approximately transversely isotropic (*Klimeš, 2015*, *2016*), the actual S waves propagate approximately along the SH and SV reference rays traced according to *Klimeš and Bulant (2015, 2017)*. We thus compare the anisotropic–ray–theory S–wave rays and anisotropic common rays with the SH and SV reference rays in Figs 9–14.

The anisotropic–ray–theory rays of the fast S wave are compared with the SH reference rays in Fig. 9, and with the SV reference rays in Fig. 10. The anisotropic–ray–theory rays of the fast S wave are very close to the SH reference rays for the deepest receivers, and are situated above them up to the third receiver below the surface. The anisotropic–ray–theory rays of the fast S wave nearly coincide with the SV reference rays up to third receiver below the surface. The anisotropic–ray–theory rays of the fast S wave are sharply bent from the second receiver below the surface to the ninth receiver above the surface, and considerably differ from the SH reference rays there. The anisotropic–ray–theory rays of the fast S wave nearly coincide with the SH reference rays from the tenth receiver above the surface, and are situated considerably above the SV reference rays there.

The anisotropic–ray–theory rays of the slow S wave are compared with the SH reference rays in Fig. 11, and with the SV reference rays in Fig. 12. The anisotropic–ray–theory rays of the slow S wave nearly coincide with the SH reference rays up to the surface receiver. The anisotropic–ray–theory rays of the slow S wave are situated above the SV reference rays for the deepest receivers, and are situated below the

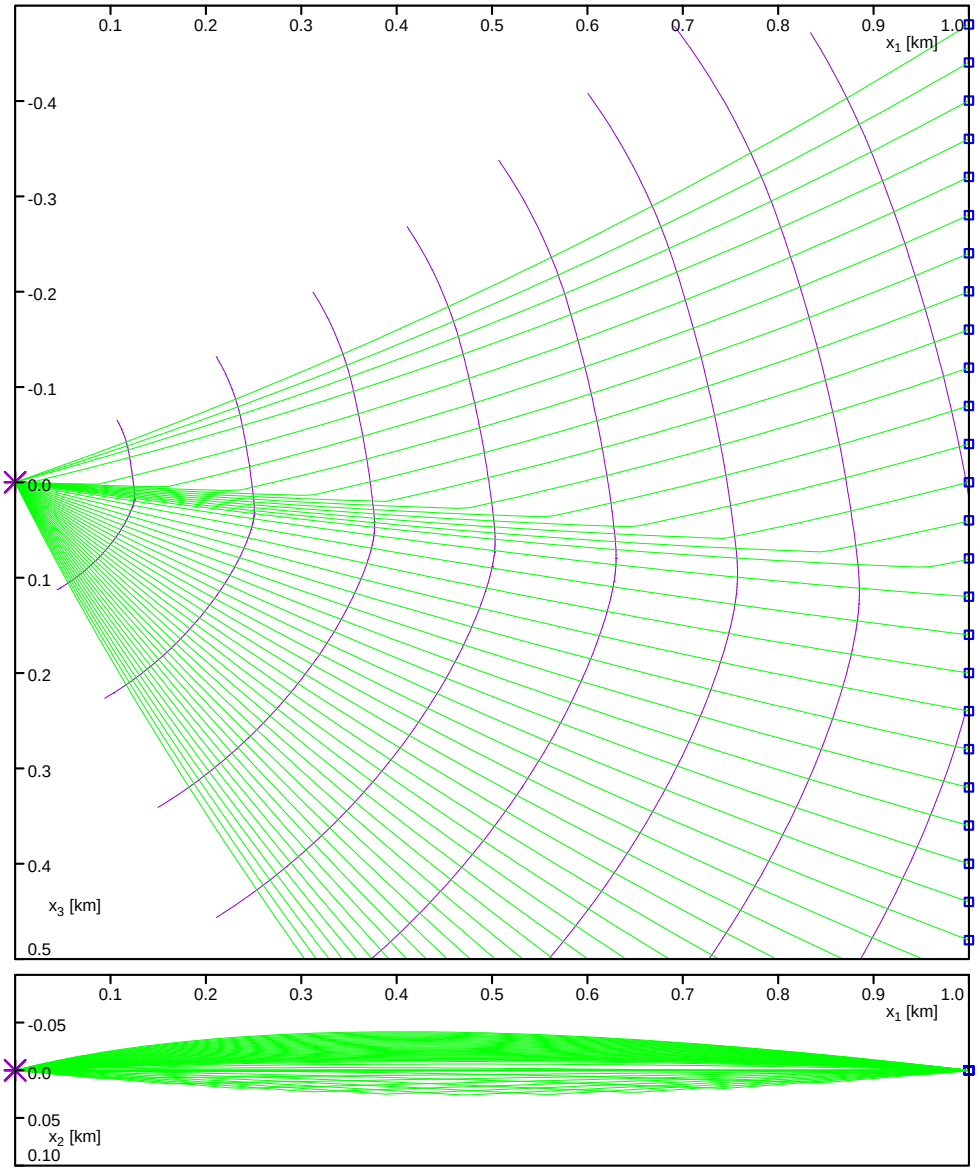

Fig. 7. Front view and top view of the anisotropic–ray–theory rays of the fast S wave. The front view is supplemented with the lines of intersection of the vertical source–receiver plane with the fast S–wave wavefronts at travel times 0.05, 0.10, 0.15, 0.20, 0.25, 0.30, 0.35 and 0.40 seconds. We can clearly observe a considerable increase of the geometrical spreading beyond the sharp bends of rays. We can simultaneously observe a considerable decrease of the wavefront curvature beyond the sharp bends of rays.

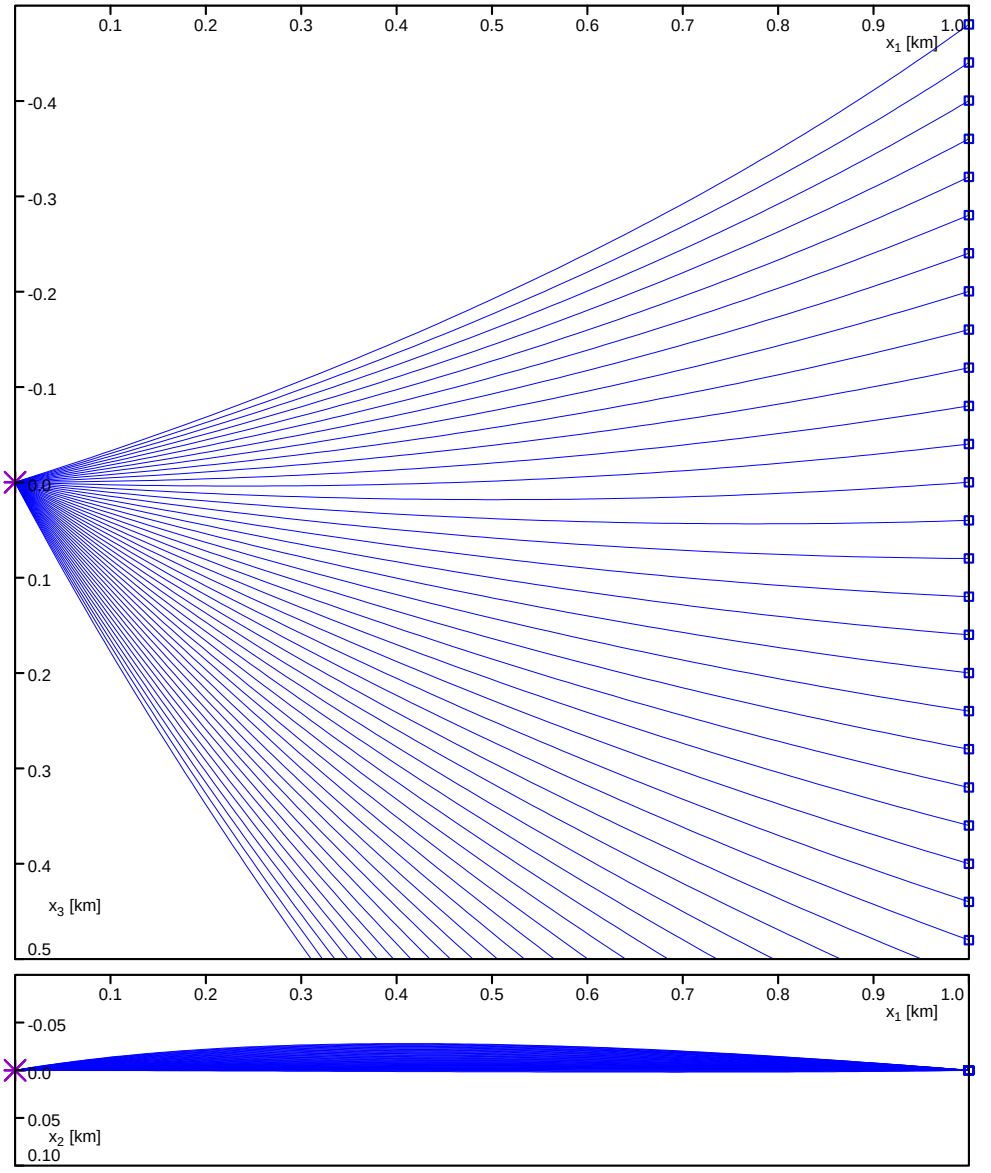

Fig. 8. Front view and top view of the anisotropic common rays. The corresponding geometrical spreading and the corresponding reference amplitude are very smooth.

SH reference rays up to the surface receiver. The anisotropic–ray–theory rays of the slow S wave display a triplication due to the sharply bent rays from the first to the third receiver above the surface. The anisotropic–ray–theory rays of the slow S wave are situated considerably below the SH reference rays from the fourth receiver above the surface, and nearly coincide with the SV reference rays there.

The anisotropic–ray–theory rays of both the fast and slow S wave thus cannot be used as the reference rays for the coupling ray theory, especially from the second receiver below the surface to the ninth receiver above the surface. They not only do not correspond to the actual wave propagation, but may also display random values of the amplitude and the KMAH index.

The anisotropic common rays are compared with the SH reference rays in Fig. 13, and with the SV reference rays in Fig. 14. The anisotropic common rays are very close to both the SH and SV reference rays for the deepest receivers. The anisotropic common rays are situated above the SH reference rays up to the seventh receiver above the surface, and are situated below them from the eighth receiver above the surface. The anisotropic common rays are situated below the SV reference rays up to the second receiver below the surface, and are situated above them from the first receiver below the surface. The anisotropic common rays are thus not situated between the SH and SV reference rays in the interval from the first receiver below the surface to the seventh receiver above the surface.

The ray paths of the anisotropic common rays reaching the receivers below the surface do not differ significantly from the SV reference rays, but the differences in geometrical spreading are considerable and result in the poor accuracy of the coupling–ray–theory seismograms calculated along the anisotropic common rays, which was demonstrated by *Klimeš and Bulant (2015, 2017)*.

6. CONCLUSIONS

We can trace the anisotropic–ray–theory rays through the split intersection singularity or close to a conical or wedge singularity of the S–wave slowness–surface, but cannot calculate the matrix of geometrical spreading. This prevents us from efficient two–point ray tracing and from calculating the amplitude and the KMAH index. We thus cannot use the anisotropic–ray–theory rays as the reference rays for the coupling ray theory in the presence of the above mentioned S–wave singularities which are more common than exceptional in anisotropic media.

However, even if there were no problems with the equations of geodesic deviation (paraxial ray equations, dynamic ray tracing equations), the S–wave anisotropic–ray–theory rays traced through the above mentioned S–wave singularities anyway do not describe the actual paths of wave propagation and do not represent reasonable reference rays for the coupling ray theory. In this case, the anisotropic common S–wave rays represent much better reference rays for the coupling ray theory. Note that the incorrect paths of the reference rays need not necessarily represent a problem in calculating the reference travel time, but usually generate incorrect reference geometrical spreading and, in consequence, incorrect reference amplitudes (*Klimeš and Bulant, 2015*, *2017*).

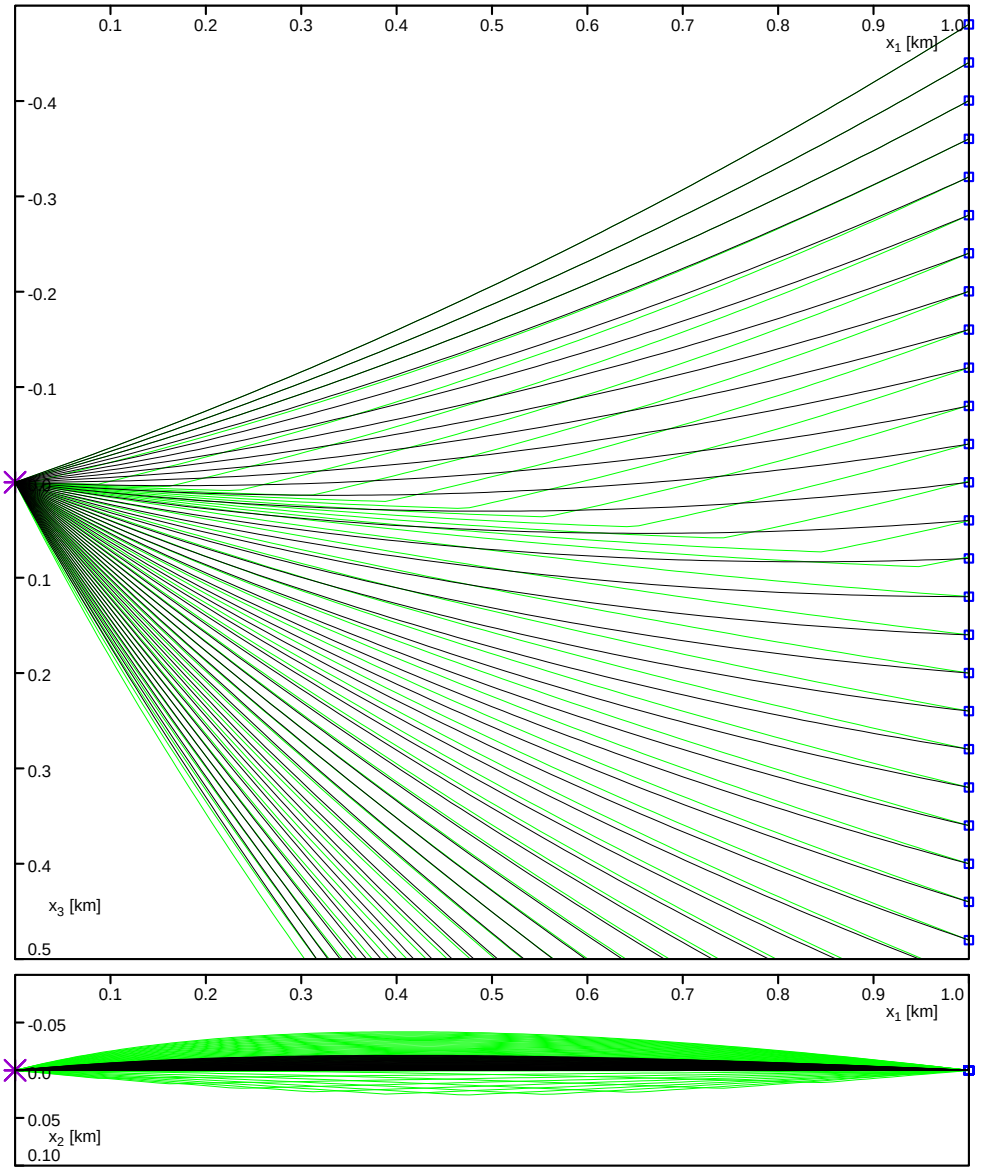

Fig. 9. Comparison of the anisotropic–ray–theory rays of the fast S wave (**green**) with the SH reference rays (**black**, plotted later on). The anisotropic–ray–theory rays of the fast S wave are very close to the SH reference rays for the deepest receivers, and are situated above them up to the third receiver below the surface. The anisotropic–ray–theory rays of the fast S wave are sharply bent from the second receiver below the surface to the ninth receiver above the surface, and considerably differ from the SH reference rays there. The anisotropic–ray–theory rays of the fast S wave nearly coincide with the SH reference rays from the tenth receiver above the surface.

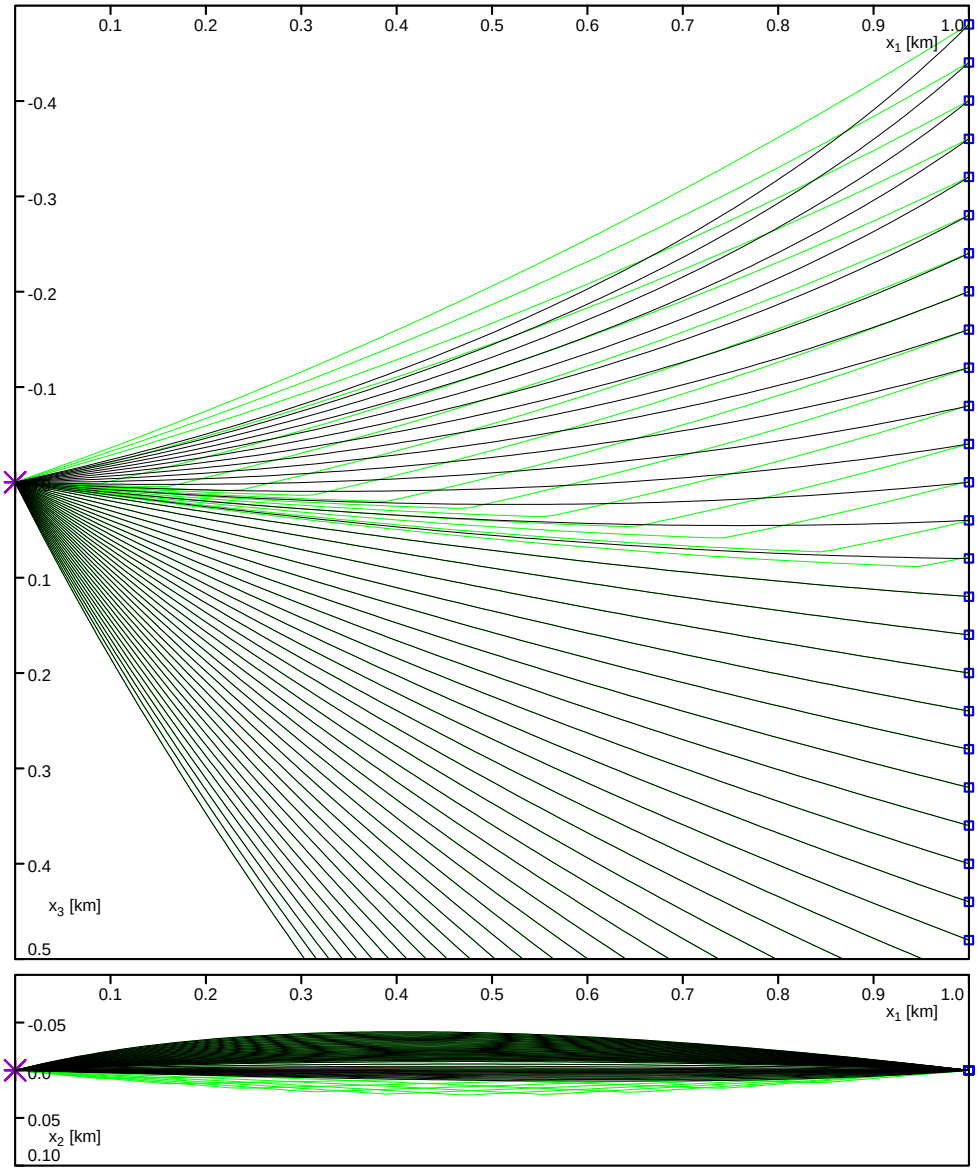

Fig. 10. Comparison of the anisotropic–ray–theory rays of the fast S wave (**green**) with the SV reference rays (**black**, plotted later on). The anisotropic–ray–theory rays of the fast S wave nearly coincide with the SV reference rays up to third receiver below the surface. The anisotropic–ray–theory rays of the fast S wave are sharply bent from the second receiver below the surface to the ninth receiver above the surface, and considerably differ from the SV reference rays. The anisotropic–ray–theory rays of the fast S wave are situated considerably above the SV reference rays from the tenth receiver above the surface.

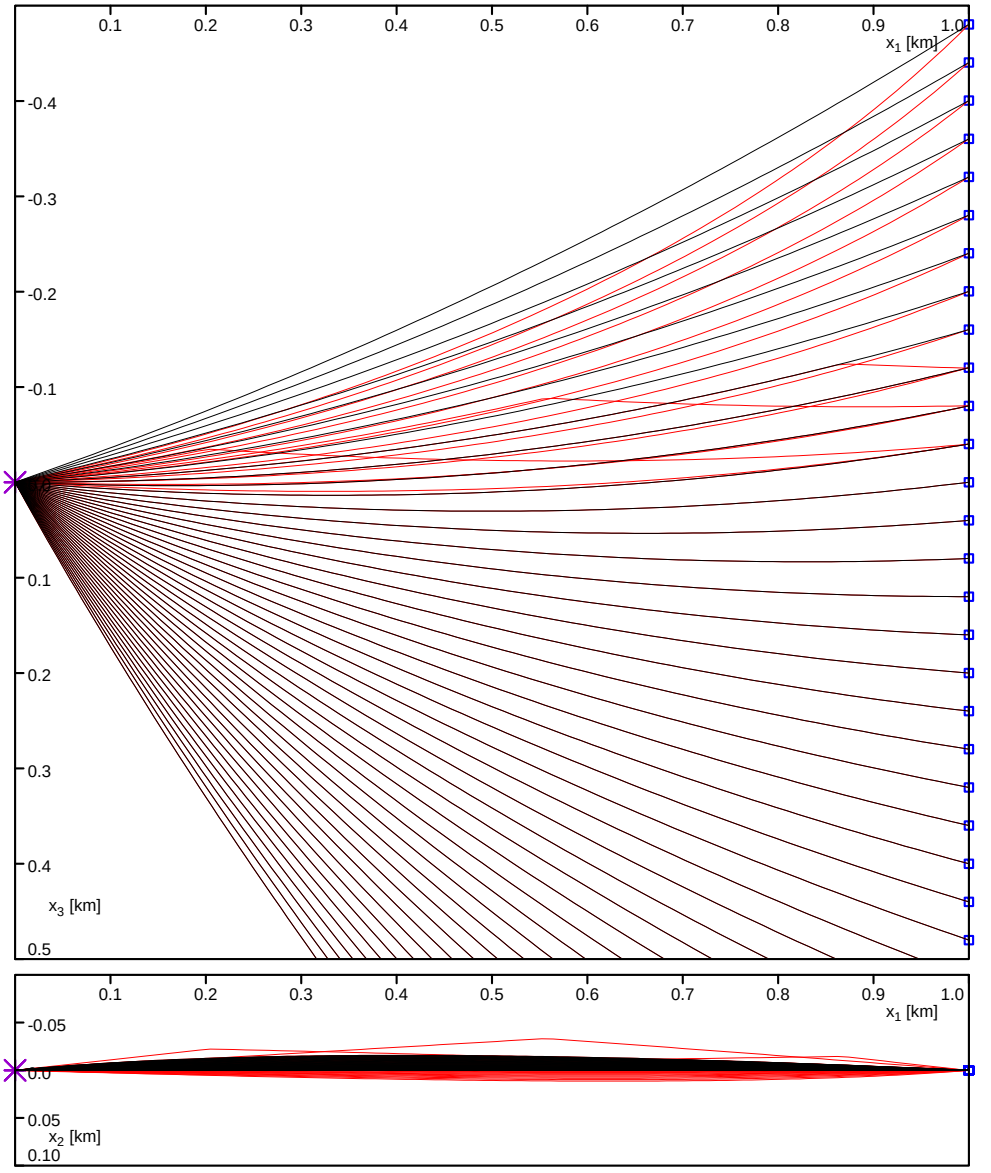

Fig. 11. Comparison of the anisotropic–ray–theory rays of the slow S wave (**red**) with the SH reference rays (**black**, plotted later on). The anisotropic–ray–theory rays of the slow S wave nearly coincide with the SH reference rays up to the surface receiver. The anisotropic–ray–theory rays of the slow S wave display a triplication due to the sharply bent rays from the first to the third receiver above the surface. The anisotropic–ray–theory rays of the slow S wave are situated considerably below the SH reference rays from the fourth receiver above the surface.

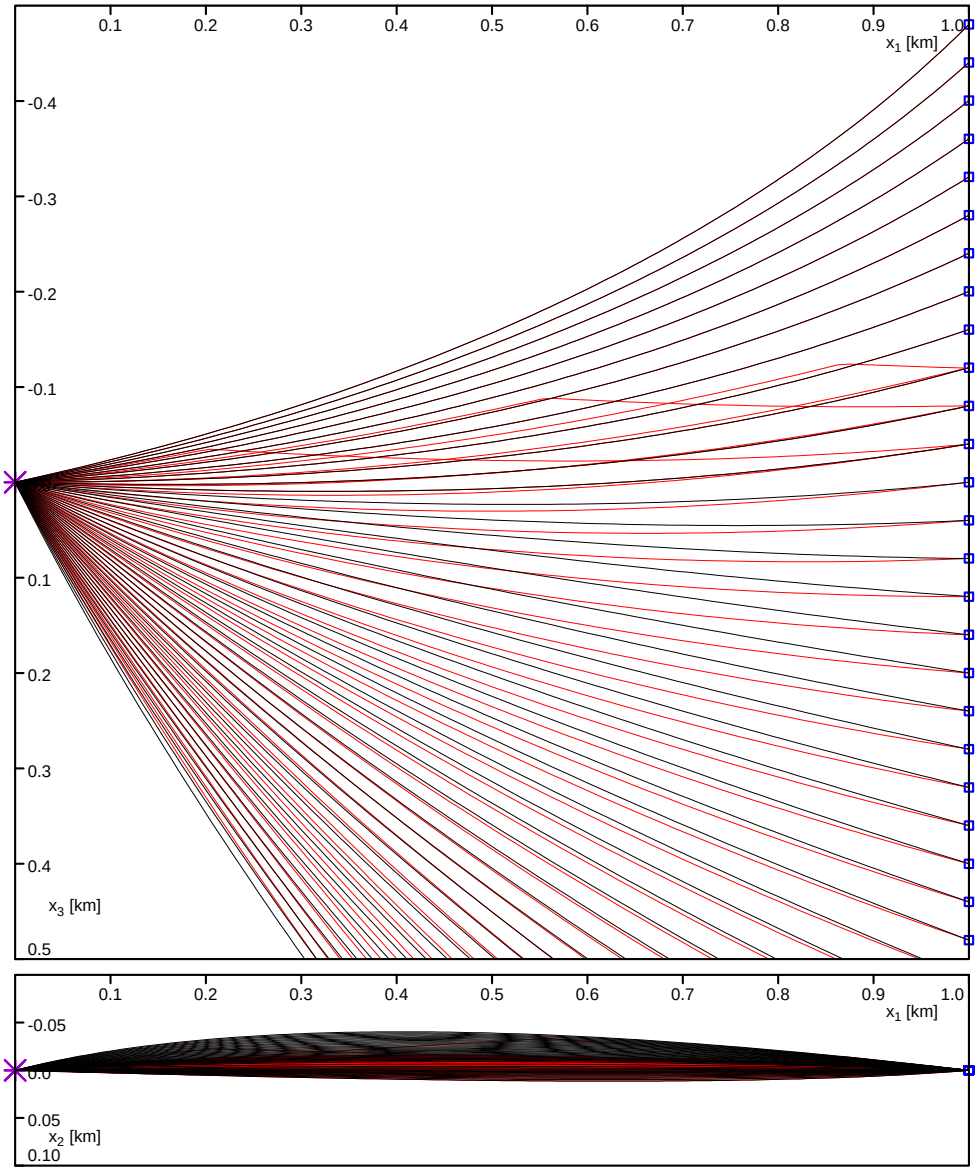

Fig. 12. Comparison of the anisotropic–ray–theory rays of the slow S wave (**red**) with the SV reference rays (**black**, plotted later on). The anisotropic–ray–theory rays of the slow S wave are situated above the SV reference rays for the deepest receivers, and are situated below the SH reference rays up to the surface receiver. The anisotropic–ray–theory rays of the slow S wave display a triplication due to the sharply bent rays from the first to the third receiver above the surface. The anisotropic–ray–theory rays of the slow S wave nearly coincide with the SV reference rays from the fourth receiver above the surface.

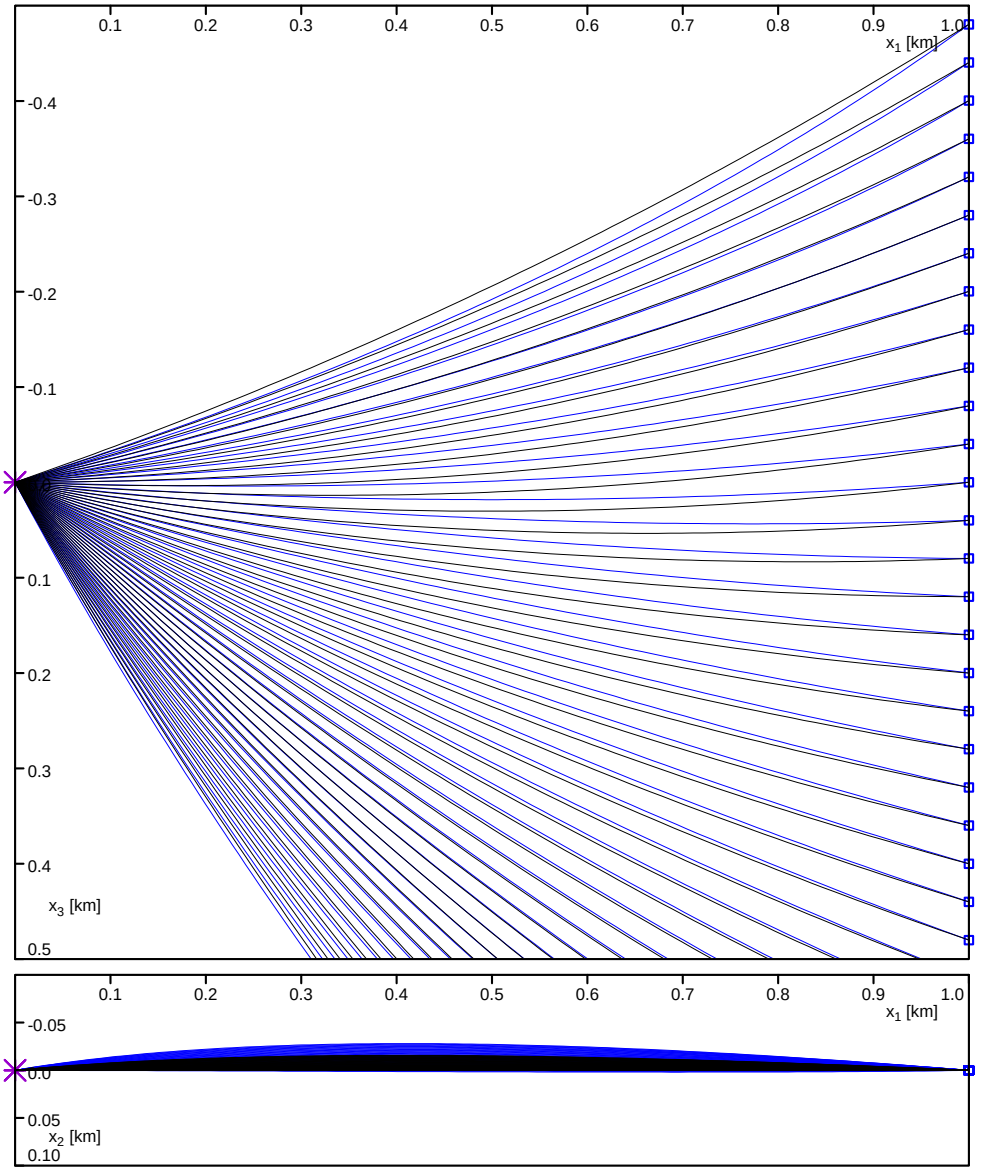

Fig. 13. Comparison of the anisotropic common rays (**blue**) with the SH reference rays (**black**, plotted later on). The anisotropic common rays are very close to the SH reference rays for the deepest receivers, are situated above them up to the seventh receiver above the surface, and are situated below them from the eighth receiver above the surface. The ray paths do not differ significantly.

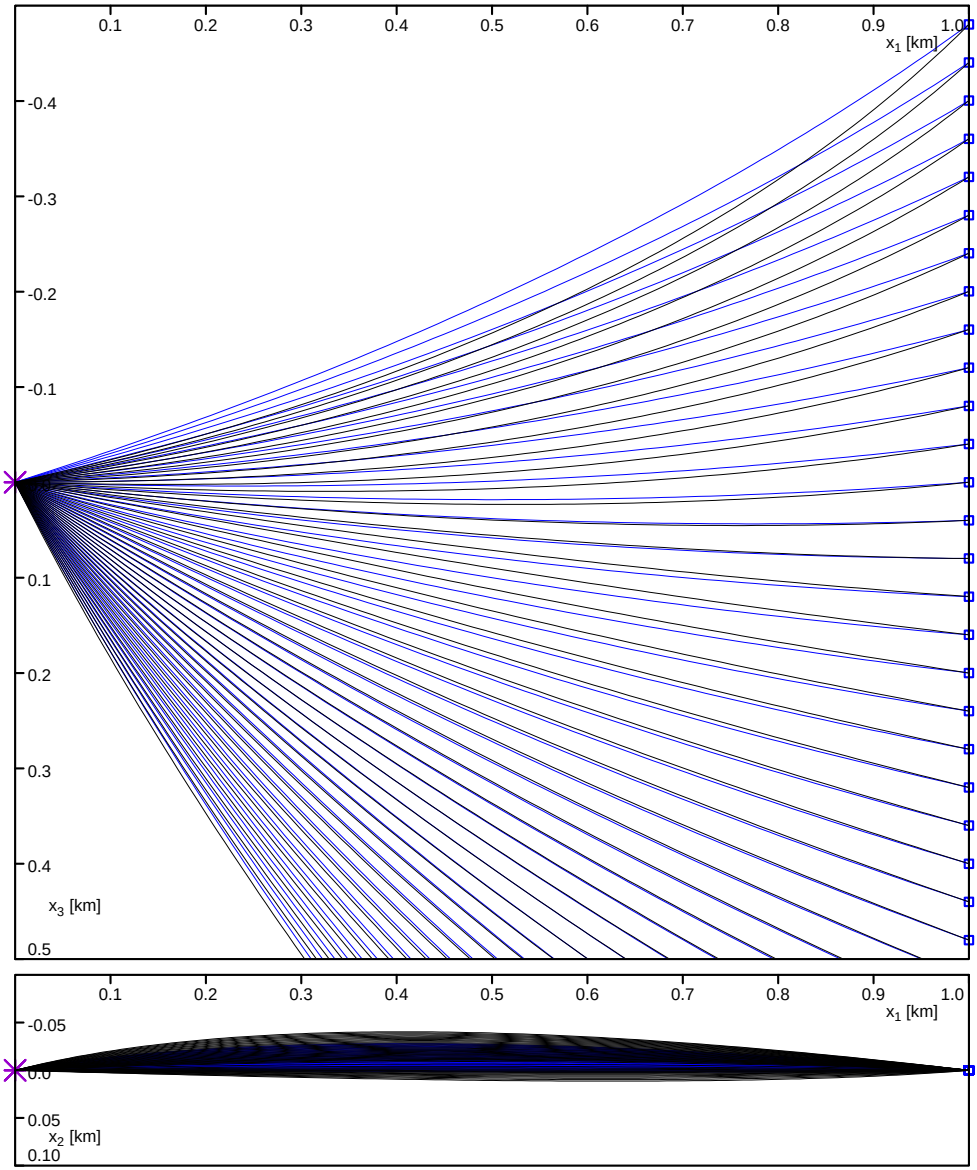

Fig. 14. Comparison of the anisotropic common rays (**blue**) with the SV reference rays (**black**, plotted later on). The anisotropic common rays are very close to the SH reference rays for the deepest receivers, are situated below them up to the second receiver below the surface, and are situated above them from the first receiver below the surface. The ray paths to the receivers below the surface do not differ significantly, but the differences in geometrical spreading are considerable and result in the poor accuracy of the coupling–ray–theory seismograms calculated along the anisotropic common rays.

If the anisotropic common S–wave rays are not sufficiently close to the actual paths of wave propagation or the corresponding common S–wave amplitudes are not sufficiently accurate for both S–wave arrivals, and the anisotropic medium is approximately transversely isotropic (*Klimeš, 2015*, *2016*), we may consider approximate SH and SV reference rays defined by *Klimeš and Bulant (2015, 2017)*. We may then apply the prevailing–frequency approximation of the coupling ray theory along these SH and SV reference rays (*Klimeš and Bulant, 2014a*).

Acknowledgements: The suggestions by Václav Vavryčuk and an anonymous reviewer made it possible for us to improve the paper considerably. The research has been supported by the Grant Agency of the Czech Republic under contracts 16-01312S and 16-05237S, by the Ministry of Education, Youth and Sports of the Czech Republic within research project CzechGeo/EPOS LM2015079, and by the members of the consortium "Seismic Waves in Complex 3–D Structures" (see "http://sw3d.cz").

References

Babich V.M., 1961. Ray method of calculating the intensity of wavefronts in the case of a heterogeneous, anisotropic, elastic medium. In: Petrashen G.I. (Ed.), *Problems of the Dynamic Theory of Propagation of Seismic Waves, Vol. 5.* Leningrad Univ. Press, Leningrad, 36–46 (in Russian, English translation: *Geophys. J. int.*, **118**(1994), 379–383).

Bucha V. and Bulant P. (Eds), 2014. SW3D–CD–18 (DVD–ROM). *Seismic Waves in Complex 3–D Structures*, **23**, 211–212 (http://sw3d.cz).

Bulant P., 1996. Two–point ray tracing in 3–D. *Pure Appl. Geophys.*, **148**, 421–447.

Bulant P., 1999. Two–point ray–tracing and controlled initial–value ray–tracing in 3–D heterogeneous block structures. *J. Seism. Explor.*, **8**, 57–75.

Bulant P. and Klimeš L., 2014. Anisotropic–ray–theory geodesic deviation and two–point ray tracing through a split intersection singularity. *Seismic Waves in Complex 3–D Structures*, **24**, 179–187 (http://sw3d.cz).

Bulant P. and Klimeš L., 2017. Prevailing–frequency approximation of the coupling ray theory along the SH and SV reference rays in a heterogeneous generally anisotropic medium which is approximately uniaxial. *Stud. Geophys. Geod.*, **61**, 513–540.

Bulant P., Pšenčík I., Farra V. and Tessmer E., 2011. Comparison of the anisotropic–common–ray approximation of the coupling ray theory for S waves with the Fourier pseudo–spectral method in weakly anisotropic models. *Seismic Waves in Complex 3–D Structures*, **21**, 167–183 (http://sw3d.cz).

Červený V., 2001. *Seismic Ray Theory.* Cambridge Univ. Press, Cambridge, U.K.

Červený V., Klimeš L. and Pšenčík I., 2007. Seismic ray method: Recent developments. *Adv. Geophys.*, **48**, 1–126.

Crampin S., 1981. A review of wave motion in anisotropic and cracked elastic–media. *Wave Motion*, **3**, 343–391.

Klimeš L., 2006. Common–ray tracing and dynamic ray tracing for S waves in a smooth elastic anisotropic medium. *Stud. Geophys. Geod.*, **50**, 449–461.

Klimeš L., 2010. Phase shift of the Green tensor due to caustics in anisotropic media. *Stud. Geophys. Geod.*, **54**, 268–289.

Klimeš L., 2014. Phase shift of a general wavefield due to caustics in anisotropic media. *Seismic Waves in Complex 3–D Structures*, **24**, 95–109 (http://sw3d.cz).

Klimeš L., 2015. Determination of the reference symmetry axis of a generally anisotropic medium which is approximately transversely isotropic. *Seismic Waves in Complex 3–D Structures*, **25**, 177–185 (http://sw3d.cz).

Klimeš L., 2016. Determination of the reference symmetry axis of a generally anisotropic medium which is approximately transversely isotropic. *Stud. Geophys. Geod.*, **60**, 391–402.

Klimeš L. and Bulant P., 2012. Single–frequency approximation of the coupling ray theory. *Seismic Waves in Complex 3–D Structures*, **22**, 143–167 (http://sw3d.cz).

Klimeš L. and Bulant P., 2014a. Prevailing–frequency approximation of the coupling ray theory for S waves along the SH and SV reference rays in a transversely isotropic medium. *Seismic Waves in Complex 3–D Structures*, **24**, 165–177 (http://sw3d.cz).

Klimeš L. and Bulant P., 2014b. Anisotropic–ray–theory rays in velocity model SC1_II with a split intersection singularity. *Seismic Waves in Complex 3–D Structures*, **24**, 189–205 (http://sw3d.cz).

Klimeš L. and Bulant P., 2015. Ray tracing and geodesic deviation of the SH and SV reference rays in a heterogeneous generally anisotropic medium which is approximately transversely isotropic. *Seismic Waves in Complex 3–D Structures*, **25**, 187–208 (http://sw3d.cz).

Klimeš L. and Bulant P., 2016. Prevailing–frequency approximation of the coupling ray theory for electromagnetic waves or elastic S waves. *Stud. Geophys. Geod.*, **60**, 419–450.

Klimeš L. and Bulant P., 2017. Ray tracing and geodesic deviation of the SH and SV reference rays in a heterogeneous generally anisotropic medium which is approximately uniaxial. *Stud. Geophys. Geod.*, **61**, 497–512.

Pšenčík I., Farra V. and Tessmer E., 2012. Comparison of the FORT approximation of the coupling ray theory with the Fourier pseudospectral method. *Stud. Geophys. Geod.*, **56**, 35–64.

Vavryčuk V., 2001. Ray tracing in anisotropic media with singularities. *Geophys. J. Int.*, **145**, 265–276.

Vavryčuk V., 2003a. Behavior of rays near singularities in anisotropic media. *Phys. Rev. B*, **67**, 054105-1–054105-8.

Vavryčuk V., 2003b. Generation of triplications in transversely isotropic media. *Phys. Rev. B*, **68**, 054107-1–054107-8.

Vavryčuk V., 2005a. Acoustic axes in weak triclinic anisotropy. *Geophys. J. Int.*, **163**, 629–638.

Vavryčuk V., 2005b. Acoustic axes in triclinic anisotropy. *J. Acoust. Soc. Am.*, **118**, 647–653.

Vinje V., Iversen E., Åstebøl K. and Gjøystdal H., 1996. Estimation of multivalued arrivals in 3D models using wavefront construction — Part I. *Geophys. Prospect.*, **44**, 819–842.